PAPER • **OPEN ACCESS**

Numerical simulations of submarine self-propulsion flows near the free surface

To cite this article: Enkai Guo *et al* 2023 *IOP Conf. Ser.: Mater. Sci. Eng.* **1288** 012055

Numerical simulations of submarine self-propulsion flows near the free surface

Enkai Guo[1], Liushuai Cao[1*], Zhiben Shen[2], Yun Wang[2]

[1] Computational Marine Hydrodynamics Lab (CMHL), School of Naval Architecture, Ocean and Civil Engineering, Shanghai Jiao Tong University, Shanghai, China.
[2] Wuhan Second Ship Design and Research Institute, Wuhan, China.
[*] Corresponding author: liushuaicao@sjtu.edu.cn

Abstract. Submarine needs to complete more tasks near the free-surface area in modern war. When sailing near the free surface, the self-propelled characteristics of the submarine and its nearby flow field will be affected by the free surface. This paper presents the research on the self-propulsion submarine near the free surface with computational fluid dynamics (CFD) method. We take the generic Joubert BB2 submarine and Marine 7371R propeller models as the research objects. The RANS method and SST k-ω turbulence model are selected to solve the turbulent flows. The volume of fluid (VOF) method is used to capture the free surface. Grid convergence study is performed based on three sets of grids with different resolution. Numerical simulations are performed under the self-propulsion cases with different submergence depths and velocities. The proportional integral (PI) controller method is proposed to obtain the self-propulsion point. The results are more accurate compared with the traditional one. It is found that with the decrease of the submergence depths, the rotating speed of the self-propelled point and the corresponding thrust increase. The study also explores the free surface effect on flow field characteristics, wave-making characteristics and vortex structures. The scientific findings provide some useful results for the self-propulsion submarines near the free surface and support the further research in the future.

1. Introduction

Modern warfare requires submarines to perform a variety of tasks in near-free-surface conditions, such as navigating in near-free-surface formations, coordinating with air forces, launching missiles, and entering or leaving ports for maintenance and resupply. Additionally, submarine listening, surveillance, and special operations capabilities in shallow coastal waters are becoming increasingly important. Modern operations require that submarines not only stick to deep-water operations, but also have near-surface combat capabilities.

Research has shown that the hydrodynamic performance and flow field characteristics of submarines change significantly when sailing near the free surface. Different research methods have been used to investigate this phenomenon, including theoretical analysis, model experiments, and computational fluid dynamics (CFD).

Theoretical analysis method is an important method. Some early scholars used slice theory and potential flow method to solve the hydrodynamic performance of the near-surface submarines [1]. Gourlay and Dawson [2] adopted the Havelock-source panel method to describe the potential flow around submarines near the free surface. It is found that the method can accurately calculate the wave resistance, pressure drag, vertical force, and trim moment of DARPA SUBOFF and Joubert submarines compared with the experimental data. The method also shows advantages in computation

speed, simplicity and robustness. However, the theoretical method is often limited by conditions and experience, such as the selection of empirical formula, which is insufficient to deal with complex flow field problems. The results of theoretical analysis often need to be verified by experimental data.

The advantage of the model experiment method is that it can create a real physical environment, therefore the results are highly reliable. Wang et al. [3] determined the hydrodynamic performance and wake characteristics of the submarine propeller when it is self-propelled near the free surface by using stereoscopic particle image velocimetry (SPIV) method. However, the model experiment method also has some shortcomings, such as the limitation of test conditions and the difficulty of flow field measurement. So, there are few documents and articles on the study self-propulsion of submarine near the free surface by using the model experiment method, which lacks sufficient data support.

With the rapid development of CFD technology, simulation software based on CFD can quickly analyze and simulate the flow characteristics of submarines. Many researchers have investigated the relative problems with different CFD methods. Lungu [4] used the detached eddy simulation (DES) method to study the flow around the self-propelled SUBOFF submarine near the free surface and mainly discussed the wave variation under different conditions. Li et al. [5] coupled the Reynolds-Averaged Navier-Stokes (RANS) equation with k-ω turbulence model to conduct the self-propulsion simulation and analyze the influence of the free surface on the performance of propeller. Carrica [6] used a general purpose CFD code REX to conduct near-surface self-propulsion simulations and study the hydrodynamics performance of submarine and propeller both in calm water and waves. Dong [7] used RANS solver to simulate the impact of long-crested waves on the self-propulsion submarines. Huang et al. [8] also used RANS method to analyze the wave-making characteristics of the near-surface submarines.

This paper presents the research on the self-propulsion submarines near the free surface. The study in this paper takes the standard Joubert BB2 submarine and Marine 7371R propeller as the research object. The RANS equation and SST k-ω turbulence model is selected. The VOF method is used to establish the free surface. Numerical simulations are conducted under the cases with different submergence depths and velocities. The linear interpolation method and the PI controller method are applied to obtain the self-propulsion points. There is no significant difference between their results. The results are compared to explore the influence of and submergence depth on submarines self-propulsion performance, flow field characteristics, wave-making characteristics and vortex structures. All of the simulations are conducted based on the CFD software STAR-CCM+.

2. Methodology

2.1. Submarine and propeller geometries

The Joubert BB2 submarine model and six-bladed propeller 7371R model were used for the self-propulsion study. They were both designed by Maritime Research Institute Netherlands (MARIN). Figure 1 shows the entire self-propulsion model and the appendages on it. The BB2 model consists of main hull, sail, sailplanes and X rudders. Table 1 shows the main parameters of the submarine and propeller models at model scale (λ=18.348) and full scale.

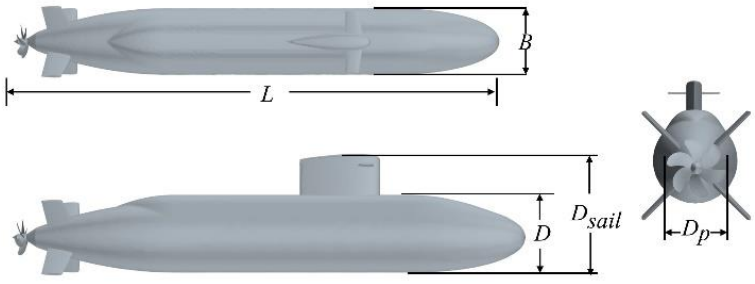

Figure 1. The submarine and propeller model.

Table 1. The main parameters of the submarine and propeller models.

Description	Symbol	Full scale value	Model scale value	Unit
Length	L	70.20	3.826	m
Beam	B	9.60	0.5232	m
Drought to deck	D	10.60	0.5777	m
Drought to sail	D_{sail}	16.20	0.8829	m
Diameter of propeller	D_p	5	0.273	m
Pitch ratio	P/D_p	0.966	0.966	-

2.2. Governing equations and turbulence model

Simulations in this study were conducted by solving Reynolds-Averaged Navier-Stokes (RANS) equations in STAR-CCM+ software. The flow is incompressible and turbulent. The governing equations of RANS method can be expressed as follows:

$$\frac{\partial \overline{u}_i}{\partial x_i} = 0 \tag{1}$$

$$\frac{\partial \overline{u}_i}{\partial t} + \overline{u}_j \frac{\partial \overline{u}_i}{\partial x_j} = \overline{f}_i - \frac{1}{\rho}\frac{\partial \overline{p}}{\partial x_i} + \nu \frac{\partial^2 \overline{u}_i}{\partial x_j \partial x_j} - \frac{\partial \overline{u_i' u_j'}}{\partial x_j} \tag{2}$$

where $\overline{u_i}$, $\overline{f_i}$ and $\bar{p}$ are the time averaged values of velocity component, force and pressure.

In this study, the SST k-ω turbulence model is selected to close the solving equations, which is proposed by Menter [9]. It uses k-ω model to deal with the flow in the boundary layer and k-ε to deal with the flow of free fluid. Its transport equations are given as:

$$\frac{\partial}{\partial t}(\rho k) + \frac{\partial}{\partial x_i}(\rho k u_i) = \frac{\partial}{\partial x_j}\left(\Gamma_k \frac{\partial k}{\partial x_j}\right) + G_k - Y_k + S_k \tag{3}$$

$$\frac{\partial}{\partial t}(\rho \omega) + \frac{\partial}{\partial x_i}(\rho \omega u_i) = \frac{\partial}{\partial x_j}\left(\Gamma_\omega \frac{\partial \omega}{\partial x_j}\right) + G_\omega - Y_\omega + S_\omega \tag{4}$$

where Γ_k, Γ_ω represent the effective diffusivity; G_k, G_ω represent the turbulent kinetic energy; Y_k, Y_ω represent the energy dissipation; S_k, S_ω represent the source item.

2.3. Free surface model

Volume of fluid (VOF) method is a moving interface tracking method based on Euler grid, which is proposed by Hirt and Nichols [10]. Its basic principle is to simulate the moving interface by defining a VOF function of the ratio between the volume of the target fluid and the grid, and calculating the function value on each cell element. VOF method is widely used in the simulation of multiphase transition. The advantage of VOF method is that it has good mass conservation characteristics and leads to high accuracy.

The free surface separates the air domain and the water domain. The volume fraction α is introduced to represent the ratio of a kind of fluid in the grid. The α=0 represents the air and α=1 represents the water. The equation of calculating the volume fraction α can be expressed as:

$$\frac{\partial \alpha}{\partial t} + \vec{u} \cdot \nabla \alpha = 0 \tag{5}$$

2.4. Computational domain and boundary conditions

The computational domain consists of two regions. The outer region is the static region and the inner region is the rotating region. The rotating region is a cylinder with a diameter of $1.32D_p$ and a height of $0.26D_p$. It completely encloses the blades and hub of the propeller. The boundary of the rotating region is defined as interface. The boundary of the static region is a cuboid. The inlet boundary is $3.18L$ away from the front nose tip of submarine which is defined as velocity inlet. The outlet

boundary is 4.18*L* away from the tail tip of submarine which is defined as pressure outlet. The top boundary is 2.09*L* away from the submarine's surface. The bottom boundary is 4.18*L* away from the submarine's surface. The bilateral boundaries are 4.18*L* away from the port or starboard. They are all defined as symmetry plane. The surfaces of body (including hull, appendages, propeller blades and shaft) are defined as no-slip wall.

As shown in Figure 2, the free surface is established parallel to the submarine's base plane (z=0 plane). The distance between the base plane and the free surface is defined as the submergence depth H. The static region is divided into air domain and water domain by the free surface.

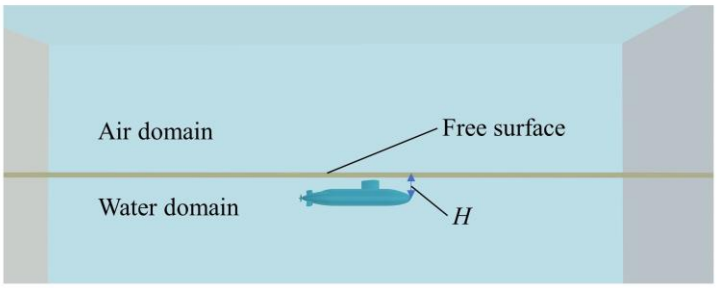

Figure 2. The computational domain.

2.5. Self-propulsion simulation method

In this study, two different methods were used to obtain self-propulsion point in order to verify the accuracy of simulation.

The first one is a traditional method which was proposed by Yang et al. [11]. The key to this method is to adjust rotating speed in order to balance the thrust of propeller and total resistance of submarine under fixed velocity. The process is as follows.

(1) There is a uniform flow with fixed speed in the computational domain. We estimate an initial rotating speed through propeller's open water performance.

(2) The numerical simulation is conducted at fixed speed and rotating speed. The thrust (T) value and resistance (D) value are monitored and noted when they are convergent.

(3) If $T>D$, reduce the rotating speed; If $T<D$, increase the rotating speed. Then we conduct the simulation again and repeat the steps above until the thrust value is equal to the resistance value.

(4) When $T=D$, the corresponding rotating speed represents the self-propulsion point at that speed. The wake fraction, thrust deduction coefficient and other self-propulsion factors can be calculated according to the resistance curve of the hull and the open water performance curve of the propeller.

However, in the realistic operating process, it is often difficult to directly obtain the self-propulsion point where the thrust value is exactly equal to the resistance value. Therefore, simulations are conducted at several rotating speeds near the self-propulsion point and the balancing point of thrust and resistance can be acquired through linear interpolation.

The other one is using a proportional-integral (PI) controller to find the self-propulsion point. A PI controller is designed to drive the propeller's rotating speed based on the error between the submarine's current speed and target speed. During the simulation, the rotating speed is not fixed but changing dynamically. The process of every step is given in Figure 3.

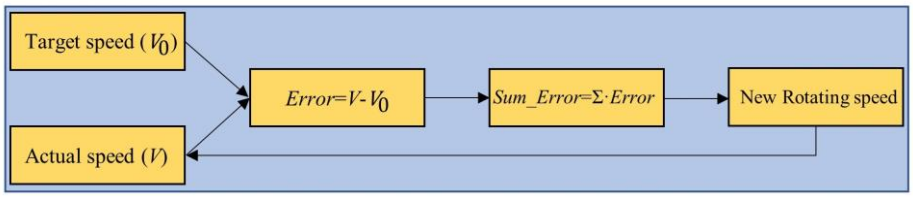

Figure 3. The process of PI controller simulation.

The general formula for the PI controller can be expressed as follows:

$$n(t) = n_0\left(1 + K_p \cdot error + K_i \cdot \sum error\right) \tag{6}$$

where $n(t)$ is the rotating speed at different times; n_0 is the initial value of rotating speed; error is the error at certain time which means submarine's target speed minus current speed here. K_p is the gain for the proportional component of the controller; K_i is the gain for the integral component of the controller.

3. Mesh generation and validation

In this study, mesh generation is mainly based on the Trimmed Mesher in both static region and rotating region. The Prism Layer Mesher is used in the boundary layer around the submarine and the propeller to simulate the fluid flow in the boundary layer more accurately. The mesh is refined in the turbulence wake region of rudders and sail. Meanwhile the mesh in far field is relatively coarser.

To verifying the mesh dependence and the accuracy of simulation, we totally established three different grids and classify them as coarse grid, medium grid and fine grid based on their basic cell sizes. Then all of the grids are used to simulate at deep depth (submergence depth *H* is big enough) in a fixed speed of 1.19m/s. The results of rotating speed and thrust at self-propulsion point are compared with the results from Kim et al. [12] as shown in Table 2. It can be noticed that all the values of other cases are well below 4% which is acceptable. The results of the case with the finest grid also don't show much superiority compared with others. So there is no need to further increase the grid size. The medium grid is finally chosen to be used for the following simulation which has an approximate 5.8 million cells. The details of the mesh in the midship section are shown in Figure 4.

Table 2. The results of mesh dependence validation.

Grid	cells (million)	points (million)	rotating speed (rpm)	δ_1 (%)	thrust (N)	δ_2 (%)
coarse	3.8	4.2	276.6	2.07	26.9	3.07
medium	5.8	6.3	275.2	1.55	26.6	1.92
fine	9.7	10.3	271.9	0.33	25.9	-0.77
Kim (2017)	-	-	271	-	26.1	-

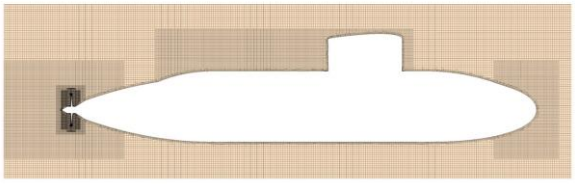

(a) Fine Grid

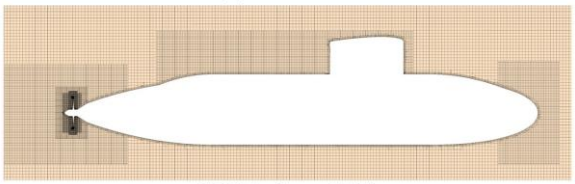

(b) Medium Grid

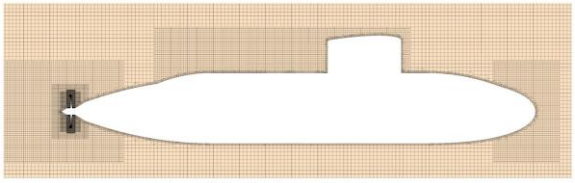

(c) Coarse Grid

Figure 4. The details of the mesh in the midship section.

4. Results and discussions

4.1. Hydrodynamic forces

Simulations were conducted in totally 8 different cases including 2 submarine velocities (1.201m/s and 1.6309m/s) and 4 submergence depth (0.5m, 0.845m, 1.0m and infinite) as is given in Table 3. In every case, both of the linear interpolation method and the PI controller method were used to obtain the self-propulsion point.

Table 3 shows the results of rotating speed (n) and thrust (T) at the self-propulsion point in corresponding cases. Obviously at the same submergence depth, higher submarine velocity corresponds to higher rotating speed and thrust. At the same velocity, deeper submergence depth corresponds to lower rotating speed. The results of the linear interpolation method and the PI controller method have the same trend. There is no significant difference between them, which proves that the simulations' accuracy.

Table 3. The results of mesh dependence validation.

case	Velocity (m/s)	Depth (m)	Traditional method		PI-controller method	
			n (r/min)	T (N)	n (r/min)	T (N)
1	1.201	0.5	310.3	37.9	310.8	38.8
2	1.201	0.845	280.7	28	282.9	29.1
3	1.201	1	278.9	27.6	280	28.1
4	1.201	infinity	277.7	27.1	277.6	27
5	1.6309	0.5	443.3	85.4	443.2	85.2
6	1.6309	0.845	386.4	54.7	386.4	54.6
7	1.6309	1	376.7	50.2	377.9	50.7
8	1.6309	infinity	372.2	47.7	372.5	47.8

4.2. Wave-making characteristics

Figure 5 shows the height of the free surface relative to the initial position under different depth conditions, that is, the wave height. The same color bar scale is used at the same velocity, which reflects the wave making characteristics at the free surface. The wave on the free surface resembles the Kelvin wave pattern well, which consists of transverse wave system perpendicular to the direction of motion and divergent wave system diagonal to the direction of motion.

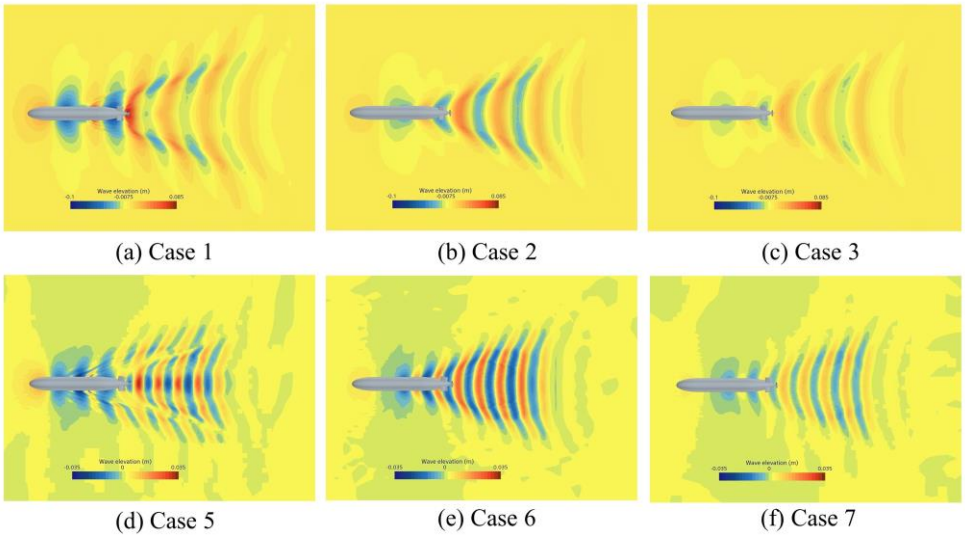

Figure 5. The waves on the free surface in different cases.

In case 1 and case 5, where the submergence depth is 0.5m, clear Kelvin wave system characteristics can be observed, especially steep divergent waves. As part of the sail and sailplanes protruding from the water, the free surface interacts with the hull to form a wave with large amplitude. In case 2 and 6, where the submergence depth increases to 0.845m. Kelvin wave system features become weak and divergent waves cannot be clearly observed. In case 3 and 7, where the submergence depth increases to 1.0m. Divergent wave system features become further weaker and the Kelvin angle decreases. In addition, due to the lower amplitude, there are some clutter wave interferences.

4.3. Flow field characteristics

Figure 6 shows the velocity nephograms at the midship section of the submarine at the velocity of 1.6309 m/s at various depths. Color bar scale is represented by dimensionless velocity. When the free surface exists, the bow flow field gradually diffuses from the front stagnation point of the submarine to the free surface in a circle, forming a wave crest; The high-velocity flow formed above the sail and sailplanes diffuses upward and backward to the free surface, forming a wave trough with large amplitude; The flow behind the sail diffuses to the rear of the submarine and merges with the flow behind the stern rudders and the flow formed by the propeller rotation, which diffuse upward to the free surface, forming a wave crest with large amplitude. They correspond to the wave-making characteristics in Section 4.2. Compared the cases (b), (c), (d) with the case (a), it is found that the flow field below the submarine is similar, while the flow field above it changes greatly. Due to Bernoulli's principle, the flow velocity increases in the area below the wave trough, forming a high-speed area. The flow velocity decreases in the area below the wave crest respectively. In addition, the existence of free surface aggravates the disturbance of the flow field near the propeller, increasing the wake velocity of the propeller and making the two wake lines generated by the propeller shift downward.

When the submergence depth is shallow, the flow near the sail interacts with the transverse waves on the free surface, generating divergent waves and other wave systems. When the submergence depth is deep, while the distance from the free surface is far, the hull can hardly affect the waveform. Therefore, the transverse waves are the main waveform.

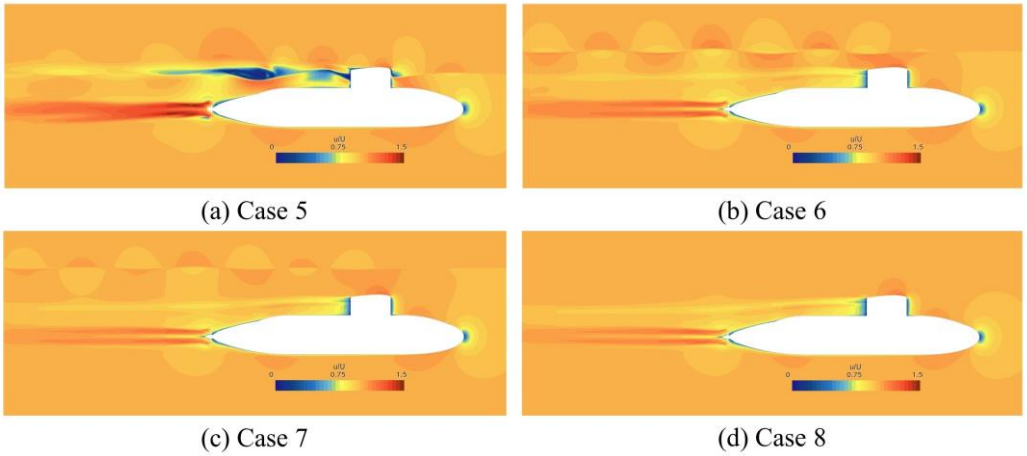

Figure 6. The velocity nephograms at the midship section in different cases.

4.4. Vortex structures

After the analysis of flow field, Q-criterion is used to analyze the vortex structure around the submarine and propeller. Q-criterion is widely used for discriminating and visualizing vortex tubes. The basic expression of Q is as follows:

$$Q = \frac{1}{2}\left(\| \Omega \|^2 - \| S \|^2 \right) \tag{7}$$

where $\Omega = 0.5\left[\nabla v - (\nabla v)^T \right]$ is the antisymmetric vorticity tensor, $S = 0.5\left[\nabla v + (\nabla v)^T \right]$ is the symmetric strain tensor.

Figure 7 shows the vortex structures visualized by Q-iso-surface under three different submergence conditions. The Q values of all the conditions are the same. The pressure field function is used for coloring. In Figure 7 (a) where the sail and sailplanes protruding from the free surface, it can be seen that the vortex structure formed behind the sail merges with the free surface, and then tends to approach the upper surface of the hull. The tip vortex behind the rudders is affected by the free surface, and the vortex tube becomes longer and thicker. The vorticity on the free surface is high. In Figure 7 (b) the tip vortex tube behind the sail tends to approach the free surface. In Figure 7 (c) the vortex structure is influenced little by the free surface.

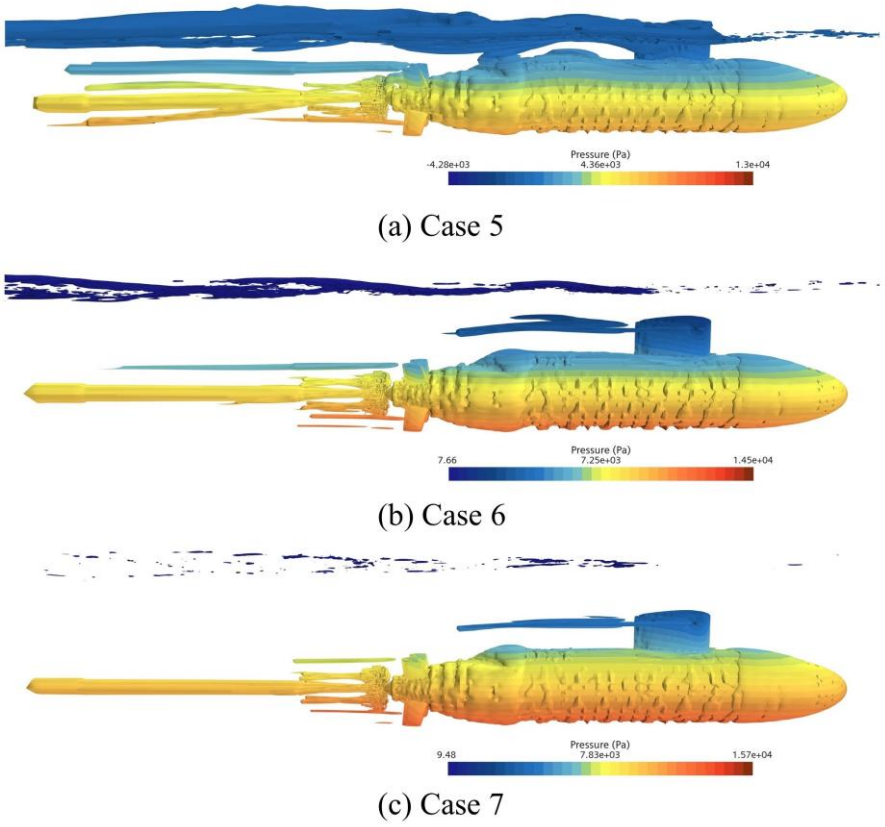

(a) Case 5

(b) Case 6

(c) Case 7

Figure 7. The vortex structures in different cases.

5. Conclusions

This study conducted the self-propulsion numerical simulations of Joubert BB2 submarine and Marine 7371R propeller through both linear interpolation method and PI controller method based on a commercial software STAR-CCM+. The main findings are described below:

(1) The self-propulsion results calculated by the PI-controller method is similar to the results calculated by the traditional method. With the decrease of the submergence depth, the rotating speed and corresponding thrust at the self-propulsion points will increase.

(2) The wave-making characteristics on the free surface are similar to Kevin waves. With the increase of submergence depth, divergent wave features become weaker and only transverse waves can be observed. Under the same velocity, the case with deeper submergence depth has the smaller amplitude, while at the same submergence depth, the case with higher velocity has greater amplitude and longer wavelength. A wave crest appears at the bow, a wave trough with large amplitude appears at the middle of the hull and a wave crest with large amplitude appears behind the propeller.

(3) The existence of the free surface changes the flow field between the free surface and the upper surface of the hull. The flow near the sail spread upward to the free surface. The interaction between the flow field and the free surface aggravates the inhomogeneity of the wake velocity behind the rudders and the propeller.

(4) When the sail protrudes from the free surface, a high vorticity field will be formed on the free surface around it. The vortex structure formed behind the sail merges with the free surface, and then tends to approach the upper surface of the hull. When the sail is below the free surface, the tip vortex behind the sail extends longer and tends to diffuse to the free surface.

This paper presents some basic research results of submarine self-propulsion in straight near the free surface. In the future, complex maneuverability tests such as steady turning tests can be investigated as further research.

Acknowledgements
This work was supported by the National Natural Science Foundation of China (52001210, 52131102), and the National Key Research and Development Program of China (2019YFB1704200), to which the authors are most grateful. The authors specially thank to Prof. Decheng Wan for his kind suggestions and supervision.

References

[1] Feng X, Jiang Q, Miao Q and Kuang X 2002 *Journal of Ship Mechanics* **02** 1-14
[2] Gourlay T and Dawson E 2015 *J. Mar. Sci. Appl.* **14** 215-224
[3] Wang L, Martin J E, Felli M and Carrica P M 2020 *Ocean. Eng.* **206** 107304
[4] Lungu A 2022 *Ocean. Eng.* **244** 110358
[5] Li P, Wang C, Han Y, Kuai Y and Wang S 2021 *Chinese Journal of Theoretical and Applied Mechanics* **53(9)** 2501-2514
[6] Carrica P M, Kim Y and Martin J E 2019 *Ocean. Eng.* **183** 87-105
[7] Dong K, Wang X, Zhang D, Liu L and Feng D 2022 *J. Mar. Sci. Eng.* **10(1)** 90
[8] Huang F, Meng Q, Cao L and Wan D 2022 *Ocean. Eng.* **250** 111062
[9] Menter F R 1994 *AIAA. J.* **32(8)** 1598-1605
[10] Hirt C W and Nichols B D 1981 *J. Comput. Phys.* **39(1)** 201-225
[11] Yang Q, Wang G, Zhang Z, Feng D and Wang X 2013 *Chinese Journal of Ship Research* **8(2)** 22-27
[12] Kim H, Ranmuthugala D, Leong Z Q and Chin C 2018 *Ocean. Eng.* **150** 102-112